Chemistry-climate model simulations of recent trends in lower stratospheric temperature and stratospheric residual circulation

Lei Wang[1] and Darryn W. Waugh[1]

Received 7 November 2011; revised 1 April 2012; accepted 3 April 2012; published 5 May 2012.

[1] Observations of the lower stratospheric temperature over the last three decades show seasonal variations in tropical trends together with spatial patterns in southern high latitude trends in late winter-spring, with regions of cooling and warming of comparable magnitude. Neither aspect is reproduced in climate models used in the Intergovernmental Panel on Climate Change's Fourth Assessment Report (IPCC AR4). Here we show that stratosphere-resolving chemistry-climate models can produce these aspects of temperature trends. However, the seasonality of temperature trends can vary greatly among simulations of the same model, and even if one ensemble member reproduces the observed seasonality in trends there may be little agreement with observations for another member. The variability in trends among model ensemble members is related to differences in trends in wave activity propagating into the stratosphere. These results suggest that the seasonality of the observed temperature trends could be the result of natural variability as well as, or instead of, a response to external forcing, and that comparison with these trends may not be a robust test of climate models.

Citation: Wang, L., and D. W. Waugh (2012), Chemistry-climate model simulations of recent trends in lower stratospheric temperature and stratospheric residual circulation, *J. Geophys. Res.*, *117*, D09109, doi:10.1029/2011JD017130.

1. Introduction

[2] Recent studies analyzing temperature measurements since 1979 have shown large spatial and seasonal variations in lower stratospheric temperature (LST) trends [e.g., *Hu and Fu*, 2009; *Lin et al.*, 2009 (LFSW2009 hereafter); *Randel et al.*, 2009; *Fu et al.*, 2010 (FSL2010 hereafter); *Free*, 2011; *Seidel et al.*, 2011; *Young et al.*, 2011]. In particular, they have shown that there are (1) significant spatial patterns in southern high latitude trends in late winter-spring, with regions of cooling and warming of comparable magnitude and (2) seasonal variations in tropical zonal mean temperature trends. Through multiple linear regression, LFSW2009 and FSL2010 have linked both (1) and (2) to changes in the stratospheric zonal mean meridional ("Brewer-Dobson," B-D) circulation, with a strengthening in the B-D circulation causing regions of dynamical warming in SH high-latitudes during August - November despite the radiative cooling by ozone depletion, and seasonal variations in the strengthening of the B-D circulation causing the variations in tropical temperature trends. Furthermore, LFSW2009 and FSL2010 have also shown that the climate models used in the Intergovernmental Panel on Climate Change's Fourth Assessment Report (IPCC AR4) could not reproduce the warming in the southern sub-polar stratosphere in late winter / early spring or the seasonal variation in tropical zonal mean trends. This was attributed to the lack of a secular trend in the B-D circulation for relevant seasons in these models.

[3] Here we aim to address several questions that arise from the above studies: First, can models with a well-resolved stratosphere and interactive stratospheric chemistry simulate the observed temperature trends? Second, is the inference that changes in the B-D circulation have caused the observed seasonal variations in high-latitude and tropical LST trends correct? Third, what is the cause of any change in the B-D circulation?

[4] We address these questions by considering simulations from stratosphere-resolving chemistry climate models (CCMs) that were performed in the second round of the Stratospheric Processes And their Role in Climate (SPARC) Chemistry-Climate Model Validation (CCMVal) activity (referred to as CCMVal-2), and evaluated in *SPARC CCMVal* [2010]. In contrast to the IPCC AR4 climate models, the CCMs include interactive stratospheric chemistry and have a full representation of radiation, dynamical, and chemical processes, and feedbacks among these processes. This means the CCMs can capture the coupling between stratospheric ozone and circulation changes, and may be better able to simulate the observed stratospheric temperature trends. We apply the analysis used by LFSW2009 and FSL2010 to these CCM simulations and compare results between models and observations as well as between model

[1]Department of Earth and Planetary Sciences, Johns Hopkins University, Baltimore, Maryland, USA.

Corresponding Author: L. Wang, Department of Earth and Planetary Sciences, Johns Hopkins University, 3400 N. Charles St., 301 Olin Hall, Baltimore, MD 21218, USA. (lei.wang@jhu.edu)

0148-0227/12/2011JD017130

Table 1. List of CCMVal-2 REF-B1 Simulations[a]

Models	Ensembles	Period
AMTRAC3 (Atmospheric Model with Transport and Chemistry 3)	1	1960–2007
CAM3.5 (Community Atmosphere Model 3.5)	1	1960–2006
CCSRNIES (Center for Climate-Systems Research – National Institute of Environmental Studies)	3	1960–2006
CMAM (Canadian Middle Atmosphere Model)	3	1960–2006
CNRM-ACM (Centre National de Recherches Météorologiques – ARPEGE Climat coupled MOCAGE)	2	1960–2005
E39CA (ECHAM4.L39(DLR)/CHEM/-ATTILA)	1	1960–2004
EMAC (ECHAM5 Middle-Atmosphere with Chemistry)	1	1960–2000
GEOSCCM (Goddard Earth Observing System – Chemistry-Climate Model)	1	1950–2004
LMDZrepro (Laboratoire de Météorologie Dynamique Zoom – REPROBUS)	3	1960–2006
MRI (Meteorological Research Institute)	3	1960–2006
Niwa-SOCOL (National Institute of Water and Atmospheric Research – Solar-Climate-Ozone Links)	1	1960–2004
SOCOL (Solar-Climate-Ozone Links)	3	1960–2006
ULAQ (Università degli Studi L'Aquila)	1	1960–2006
UMETRAC (Unified Model with Eulerian Transport and Atmospheric Chemistry)	1	1960–2000
UMSLIMCAT (Unified Model – SLIMCAT)	1	1960–2004
UMUKCA-METO (Unified Model / U. K. Chemistry and Aerosols Module – Met Office)	1	1960–2007
UMUKCA-UCAM (Unified Model / U. K. Chemistry and Aerosols Module – University of Cambridge)	1	1950–2006
WACCM (Whole-Atmosphere Chemistry-Climate Model)	4	1960–2005

[a]See *Morgenstern et al.* [2010] for details.

simulations. Results are presented for all CCMs in the CCMVal-2, but we focus primarily on simulations by the Canadian Middle Atmosphere Model (CMAM) [*de Grandpré et al.*, 2000; *Scinocca et al.*, 2008, 2009] that illustrate the key results.

[5] The data, models, and methods of analysis are described in the next section. In section 3 we compare the analysis of the trends in CMAM simulations with that of observations. The dynamics driving these trends is discussed in section 4. The trends in all CCMVal-2 simulations are analyzed in section 5. Concluding remarks are in section 6.

2. Data, Models and Analysis

[6] In this study we examine trends in monthly mean lower stratospheric temperature, total column ozone (TOZ), and meridional eddy heat flux (EHF) from multiple CCMs and observational analyses/reanalyses.

[7] The observational temperature data used are the MSU/AMSU lower stratosphere channel brightness temperature provided by the Remote Sensing System (version 3.3 updated in January 2011, available at www.remss.com). The horizontal resolution of these temperature data is 2.5 2.5 . The weighting function of this LST channel peaks at around 80 hPa with half maxima at 140 hPa and 40 hPa.

[8] The observed ozone data used are the monthly total column ozone compiled from a variety of satellite-based instruments by Bodeker Scientific (version 2.7, available at http://www.bodekerscientific.com/data/total-column-ozone [*Bodeker et al.*, 2005; *Müller et al.*, 2008; *Struthers et al.*, 2009]). The horizontal resolution is 1 longitude by 1.25 latitude. Data gaps are found in June 1979, June and July 1993, May 1994, and February, May, June, and August 1995, which are filled by interpolation. This interpolation does not have any significant impacts on the large scale pattern of the total column ozone that is investigated in this paper.

[9] NCEP/NCAR reanalysis [*Kalnay et al.*, 1996] daily velocity and temperature are used to calculate the monthly EHF. The EHF is used as a proxy of the wave activity entering the stratosphere. It is then used to diagnose changes in the stratospheric residual circulation, and to attribute temperature trends due to circulation changes. We use the cumulative eddy heat flux (CEHF), defined as the three-month (current and previous two) mean of the EHF. *Newman et al.* [2001] showed that the polar mean temperature is connected to eddy heat fluxes integrated over the preceding two months, and CEHF is a more appropriate diagnostic of the impact of wave activity entering the stratosphere than EHF. Previous studies calculated CEHF at 150 hPa [LFSW2009] or the average between 50 hPa and 10 hPa [*Ueyama and Wallace*, 2010; FSL2010], but here we calculate CEHF at 100 hPa in order to compare with CCMs (the EHF is only archived on this level in CCMVal-2). However, the results are qualitatively robust for different definitions of this proxy, tested with MSU LST and NCEP/NCAR EHF (not shown).

[10] We examine the output from CCM simulations of the CCMVal-2 REF-B1 scenario [*Morgenstern et al.*, 2010]. This scenario covers 1960 to 2006 and was designed to simulate the recent climate by imposing observed sea surface temperature (SST), greenhouse gases (GHGs), ozone depleting substances (ODSs), aerosol surface area densities, volcanic eruptions, solar variability, and the quasi-biennial oscillation (QBO). There were 18 CCMs in CCMVal-2 that performed REF-B1, with several performing multiple simulations (see Table 1). Combined together there are 32 REF-B1 simulations. The representation of QBO varies among these models: four models generate a spontaneous QBO, ten models have a imposed QBO, and the remaining four have no QBO [*Morgenstern et al.*, 2010]. These deviations from the specification of REF-B1 are not thought to impact much the results of this study, as the QBO is more likely to impact LST over interannual (instead of multi-decadal) time scales [e.g., *Seidel et al.*, 2011]. Detailed description of the REF-B1 scenario and all CCMs can be found in *Morgenstern et al.* [2010] [see also *SPARC CCMVal*, 2010].

[11] Analysis is performed on all 32 REF-B1 simulations, but we focus primarily on simulations of the CMAM. CMAM performed well in the CCMVal-2 evaluation [*SPARC CCMVal*, 2010] and there are three CMAM REF-B1

simulations in the CCMVal-2 archive. The differences among these ensemble members are typical of the differences found among ensemble members for other CCMs (and also the differences among CCMs). This version of CMAM is an extension of the Canadian Centre for Climate Modeling and Analysis (CCCma) third generation coupled general circulation model (CGCM3) with a vertically expanded domain. The corresponding version of the CGCM3 has been used extensively for the Intergovernmental Panel on Climate Change's Fourth Assessment Report (IPCC AR4). As well as the vertical extension of the model lid from 1 hPa (50 km) to 0.0007 hPa (100 km), CMAM also incorporates an interactive stratospheric chemistry module and a comprehensive middle-atmosphere radiative transfer scheme. Note that other CCMVal-2 reference and sensitivity simulations of CMAM use an interactive dynamic ocean [e.g., *Scinocca et al.*, 2009; *McLandress et al.*, 2010, 2011], but the REF-B1 simulations use prescribed, observed SSTs as required by the scenario.

[12] The same fields as considered in the observational data sets are examined in the CCMs. The LST field is obtained from the CCMs by applying the MSU/AMSU weighting function (also known as averaging kernel) to the temperature field. We also examine the simulated trends in the vertical component of the Transformed Eulerian Mean residual velocity w^* and lower stratospheric ozone.

[13] In both the observations and CCMs we consider trends over the period 1979–2006. This period is chosen to ensure the quality of the observed data (SH observations are of poorer quality before 1979) and to incorporate the CCM simulations (most simulations end in 2006). Following FSL2010, the fields (with the exception of EHF) are averaged (weighted by area) over three latitudinal bands: 20 N–20 S (hereafter referred to as the Tropics) and 40 N/S–82.5 N/S (hereafter referred to as NH/SH high latitudes). EHF is averaged over 40–90 N/S.

[14] The trends in observed and modeled quantities are calculated using linear regression. Trends in the CEHF are used to estimate the high-latitude LST trends due to changes in stratospheric dynamics [e.g., LFSW2009; FSL2010]. Following these earlier studies, the "dynamical component" of the high latitude LST trend is defined as the part that is congruent with the CEHF trend, i.e., the regression of the detrended LST temperature on the detrended CEHF index times the index trend. FSL2010 apply the calculation to NH and SH high latitudes separately to obtain the dynamical components of the NH / SH LST trends, and then average them to get the dynamical contribution of the high latitude LST trend. However, we have found that this method is sensitive when the polar stratospheric temperature-wave activity relation breaks down (i.e., when the LST and CEHF time series become uncorrelated or even negatively correlated). To avoid such sensitivity, the NH and SH CEHF trends are averaged first to derive the dynamical component of the high-latitude LST trend and the NH / SH LST dynamical components are calculated by the relative contribution of their corresponding CEHF trends to the combined CEHF trend. In most cases, these two methods produce similar results. We consider the magnitude of the CEHF so that the quantity is positive in both hemispheres, and an increasing trend corresponds to increasing wave activity.

[15] The statistical significance of trends is evaluated using the Student's t-test, typically at the 5% significance level (95% confidence interval). It worth noting that the classic one-sample t-test usually provides confidence intervals that distinguish individual trends from zero (e.g., as in Figure 1) but are not a direct measure to distinguish trends from two data sets. The latter can be properly assessed using the two-sample t-test [e.g., *Lanzante*, 2005]. To test whether the seasonality of trends is statistically significantly different for two data sets we apply the two-sample t-test to the amplitude (maximum minus minimum) of the seasonal cycle of the trend differences.

3. Temperature Trends in CMAM Simulations

[16] We now examine whether stratosphere-resolving CCMs can reproduce the observed temperature trends. Before presenting the results from all CCMs (in section 5), we focus first on simulations from CMAM. There are three CMAM REF-B1 simulations in the CCMVal-2 archive, but for space consideration we focus on only two of these, CMAM-2 and CMAM-3, which illustrate the differences that can occur between simulations that *differ only in their initial conditions*. For the most part, we repeat the analysis of FSL2010 for CCM data and observations, except we use a slightly different period (1979–2006) and slightly different analysis of the EHF (as described in section 2).

[17] As has been reported in many previous studies, observations show annual-mean cooling trends of LST at most latitudes, but with the magnitude and seasonality varying with latitude (e.g., Figures 1a–1d) [*Hu and Fu*, 2009; LFSW2009; *Randel et al.*, 2009; FSL2010; *Free*, 2011; *Seidel et al.*, 2011; *Young et al.*, 2011]. The CMAM simulations also show this general cooling trend, but the seasonality of the trends differs among simulations, see Figures 1e–1l. The seasonality of CMAM-2 trends (Figures 1e–1h) is generally similar to that observed (compare with Figures 1a–1d), but the seasonality of CMAM-3 trends (Figures 1i–1l) is often opposite to that observed. First, CMAM-3 has relatively strong cooling trend in tropics in March, when minimum cooling is observed (and in CMAM-2); and this contrast occurs similarly in October (Figures 1a, 1e, and 1i). Second, the CMAM-3 warming trend in boreal winter is delayed, by two months, to March, when the observed and CMAM-2 cooling trend is most evident in NH high latitudes (Figures 1c, 1g, and 1k). As discussed below, there is a strong anti-correlation between high latitude and tropical trends (compare Figures 1a, 1e, and 1i with Figures 1b, 1f, and 1j; correlation coefficients are 0.56, 0.58, 0.84, respectively), which FSL2010 related to the dynamical effects of trends in the meridional circulation.

[18] The observed cooling trends are statistically significant during July–January at tropics and in most months at high latitudes except during winter (and early austral spring), when strong planetary wave activity generates large interannual variability in polar temperatures (see confidence intervals in Figure 1 indicated by thin curves). Although the magnitudes of the simulated and observed trends are similar, the simulated trends have larger confidence intervals. This is related to slightly larger interannual variability in the simulations. The two-sample t-test is used to test the statistical

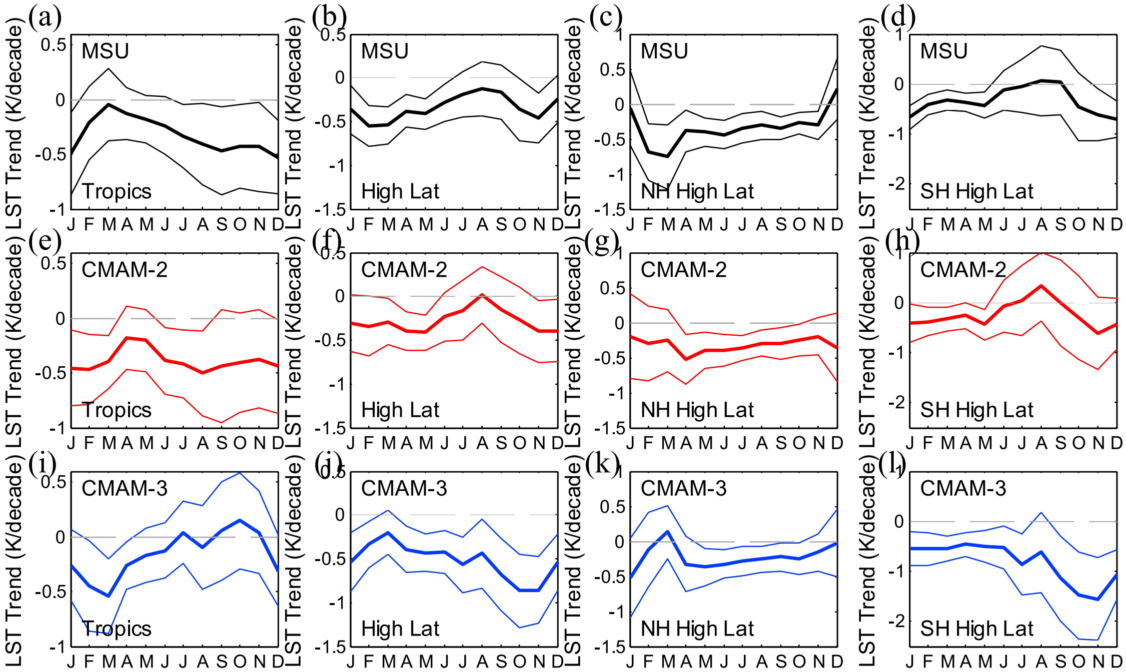

Figure 1. Observed (MSU) zonal-mean LST monthly trends (thick) and confidence intervals (thin; 5% significance level based on *t*-test) for 1979–2006 averaged over latitude bands (a) 20 S–20 N, (b) 40 N/S–82.5 N/S, (c) 40 N–82.5 N, and (d) 40 S–82.5 S. Similar to Figures 1a–1d but for CCMVal-2 REF-B1 simulations (e–h) CMAM-2 and (i–l) CMAM-3.

significance in the differences between the observed and simulated trends. It is found that the seasonality is statistically indistinguishable between MSU and CMAM-2 tropical LST trends, but is significantly different between CMAM-3 and either of above (not shown).

[19] There are large zonal variations in the observed (MSU) high latitude temperature trends during winter and spring, and the zonal-mean trend is the residual of regional warming and cooling trends [e.g., *Hu and Fu*, 2009; LFSW2009; FSL2010]. Using multiple linear regression, LFSW2009 attributed the SH high latitude trend patterns to a combination of ozone-depletion-induced radiative cooling, and dynamical warming due to the acceleration of the BD circulation. For example, the trend in SH LST in late winter and early spring can be characterized by a zonal wave number-1 structure, with regions of comparable warming and cooling, see Figures 2a and 2b. The ozone depletion intensifies over most regions poleward of 45 S during September–October (Figures 2c and 2d), as does the associated radiative cooling. As described in detail in LFSW2009, there is a large shift in the phase of the wave-1 structure of SH LST trend between September and October: The warming branch of this dipole is located at 120 E on the edge of Antarctic in August and September, and turns to 120 W in October. The warming due to circulation changes overcompensates the radiative cooling in these regions, resulting in the overall warming trend mentioned above (Figures 2a and 2b) [see also LFSW2009].

[20] As in the zonal-mean trends, CMAM-2 agrees with the observed zonally asymmetric trends better than CMAM-3 (comparing Figures 2e and 2f and Figures 2i and 2j with Figures 2a and 2b). The agreement with observations is, however, not perfect: CMAM-2 does not capture the phase of the wave-1 structure in September, and there are differences in spatial variations of the TOZ trend (Figure 2g). However, the agreement with observations is much better than for CMAM-3. There is no area of significant warming over SH high latitudes in CMAM-3 (Figures 2i and 2j) and CMAM-3 overestimates the ozone depletion trend (Figures 2k and 2l). Both the lack of dynamical warming (see below) and overestimate of the ozone depletion contribute to the large zonal-mean cooling trend in CMAM-3.

[21] Despite the statistically significant trends in both warming and cooling regions (green curves in Figures 2a, 2b, 2e, and 2f), there is near cancellation of the warming and cooling, resulting in weak zonal-mean high-latitude trends in September and October in observations and CMAM-2 (see Figures 1d and 1h). The linear regression analysis by FSL2010 also shows that the radiative cooling component (associated with ozone depletion) and the dynamical warming component (associated with strengthening of the B-D circulation) of the SH zonal mean LST trend are statistically significant (or marginally significant at the 5% level by *t*-test) by either alone in September and October when the total SH LST zonal mean trend is close to zero (and thus statistically insignificant).

[22] As discussed in the introduction, analysis in LFSW2009 and FSL2010 showed that the IPCC AR4 climate models do not reproduce the observed seasonality of zonal-mean trends or zonal asymmetries in trends at southern high latitudes. We have shown above that at least one of the CCM simulations (CMAM-2 REF-B1) is able to capture seasonal variations in the MSU LST trends. Next we will examine whether, as proposed by FSL2010, a change in the B-D circulation contributes to the seasonality.

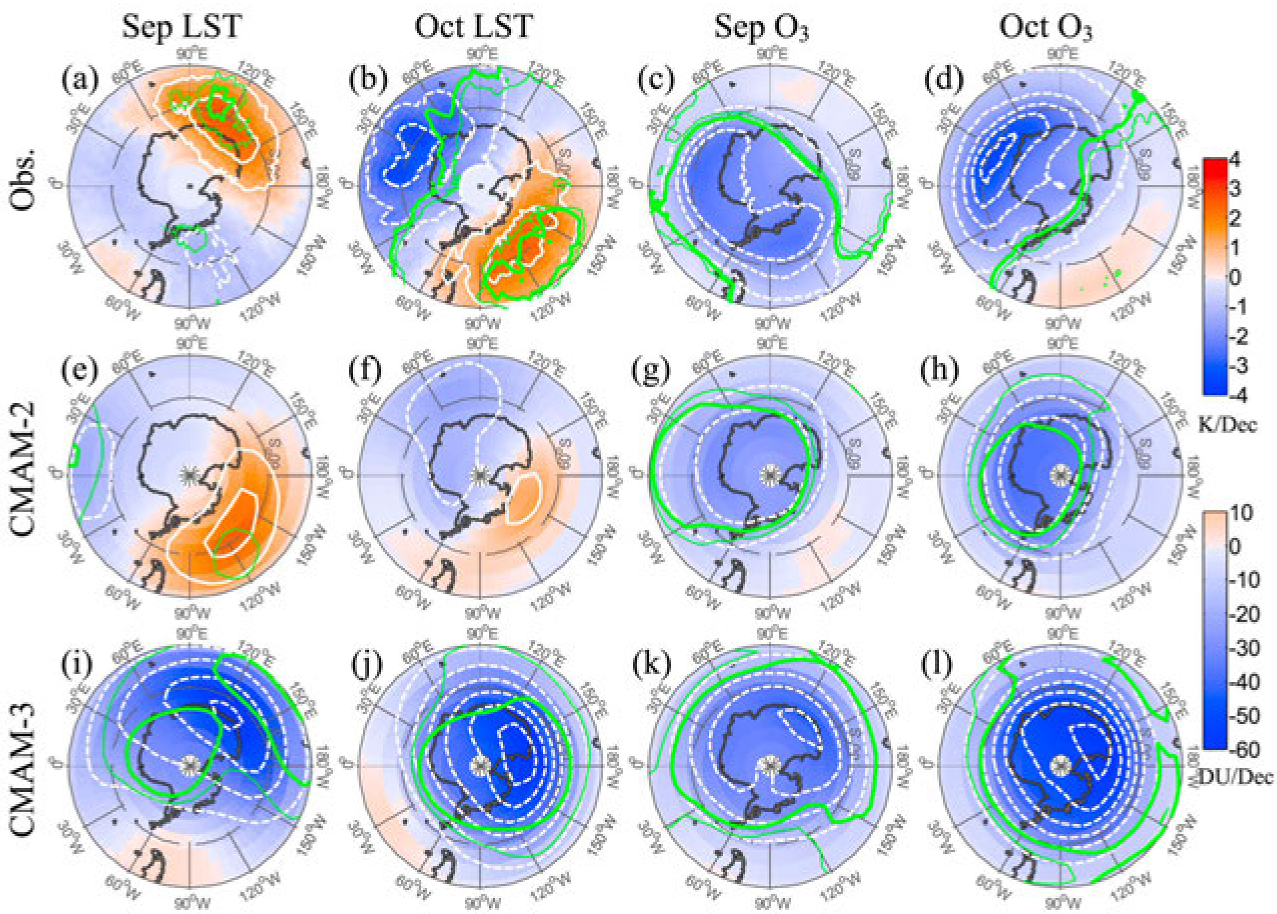

Figure 2. Maps of observed (a, b) SH LST (MSU) and (c, d) TOZ (Bodeker Scientific) 1979–2006 trends for September and October. Similar to Figures 2a–2c but for CCMVal-2 REF-B1 simulations (e–h) CMAM-2 and (i–l) CMAM-3. Contour (in white) interval is 1 K/decade for LST and 10 DU/decade for TOZ. Green contours represent the statistical significance at 10% (thin) and 5% (thick) levels based on *t*-test.

[23] The seasonality is also similar between NCEP and CMAM-2 CEHF trends (Figures 3a and 3d). On the other hand, CMAM-3 SH CEHF trends are negative from May to December, and during these months the combined high latitude CEHF trends are remarkably different from the NCEP and CMAM-2 trends (Figure 3g). The statistical significance of the differences in the seasonality between NCEP and CMAM CEHF trends can be tested using the method applied on those of the tropical LST trends above. Again, the seasonality is indistinguishable between NCEP and CMAM-2 SH or combined high latitude CEHF trends but statistically different between CMAM-3 and either of NCEP and CMAM-2 (not shown). The seasonality of NH CEHF trends is relatively similar and thus statistically indistinguishable between NCEP and CMAM simulations (not shown).

[24] The dynamical components of the high-latitude LST trends (Figures 3a, 3d, and 3g) show similar seasonality to their CEHF trends (Figures 3b, 3e, and 3h). The (combined) high latitude dynamical warming in August–October is dominated by the enhanced SH wave activity in observations (Figure 3b), which is captured by CMAM-2 albeit one month earlier (Figure 3e). Consistent with the CEHF trends, the LST high latitude dynamical component in CMAM-3 show pronounced cooling in these months (Figure 3h). In the observations, the near-zero trends in March and April (Figure 3b) are due to the cancellation between the weakening NH wave activity and strengthening SH wave activity (Figure 3a). The CMAM-2 high latitude dynamical component also shows near-zero trends in these two months but its seasonal minimum occurs in May, with dynamical cooling that is mainly due to overestimated weakening in its NH wave activity (Figures 3d and 3e). The CMAM-3 high latitude dynamical component, however, shows dynamical warming (strongest throughout the year) in April (Figure 3h). Observed strengthening of wave activity in both the NH and SH contributes to the dynamical warming in January, while CMAM-2 shows weak dynamical warming and CMAM-3 shows weak dynamical cooling (Figures 3b, 3e, and 3h).

[25] There is a high anti-correlation between the observed seasonal cycles of the dynamical high latitude LST trend and tropical LST trend ($r =$ 0.84), and the high latitude LST trend dynamical contribution explains 72% of the seasonal variation of the tropical LST trend (Figure 3c) [FSL2010]. This strong link also occurs in the CMAM simulations, even

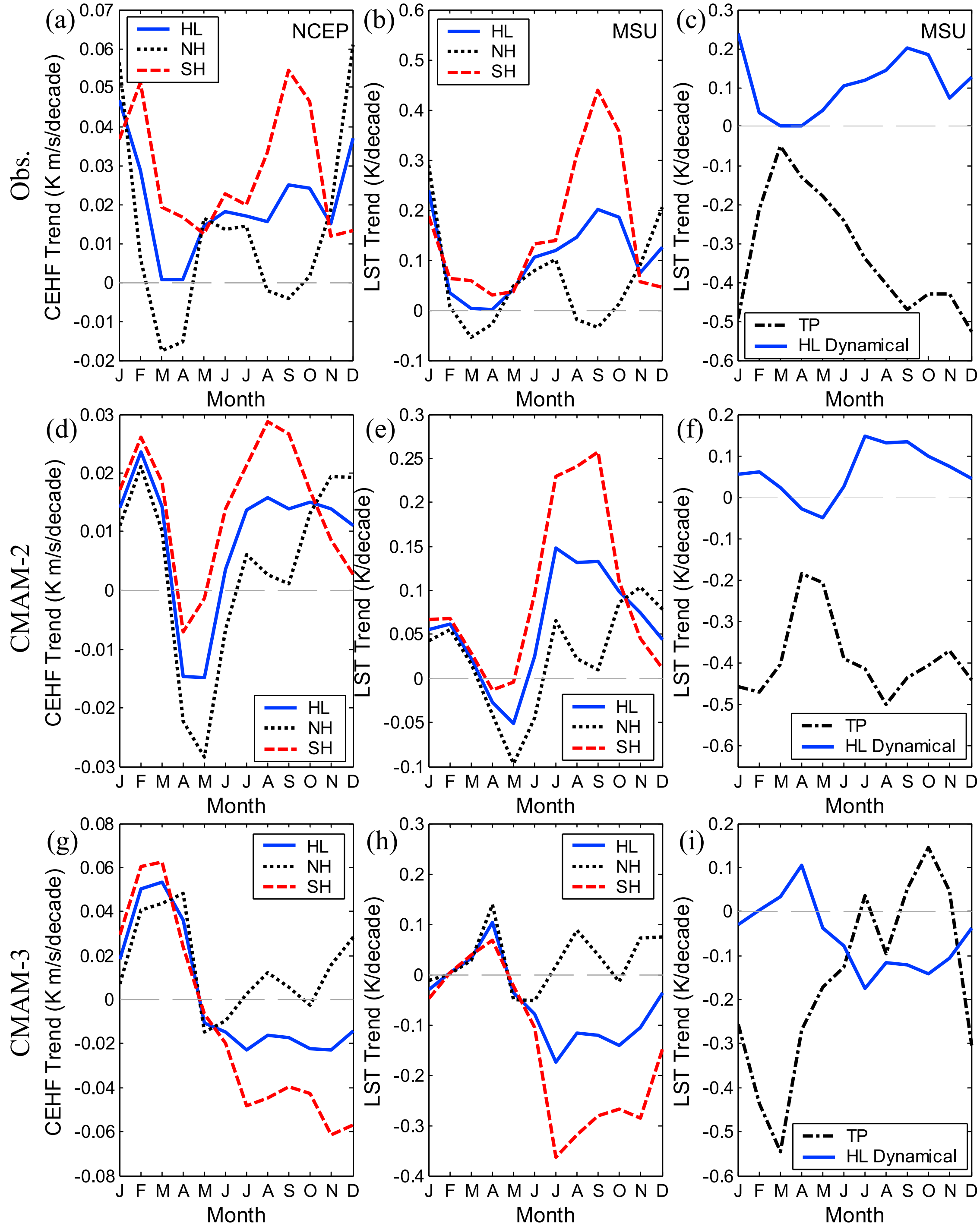

Figure 3. Seasonal variations in the observed zonal mean trends of (a) NCEP high latitude (40 N/S–90 N/S) CEHF magnitude; (b) MSU high latitude (40 N/S–82.5 N/S) dynamical LST; and (c) MSU tropical (20 S–20 N) and high latitude (40 N/S–82.5 N/S) dynamical LST. Similar to Figures 3a–3c but for CCMVal-2 REF-B1 simulations (d–f) CMAM-2 and (g–i) CMAM-3. SH trends are in red dashed, NH trends in black dotted, combined high latitude trends in blue solid, and tropical trends in black dash-dotted.

though CMAM-3 shows distinct seasonality in LST trends. There is a high anti-correlation between the high latitude dynamical LST and tropical LST trends for both CMAM-2 (r = 0.75) and CMAM-3 (r = 0.81), see Figures 3f and 3i.

[26] In summary, the above analysis shows that two simulations of the same CCM, which differ only in their initial conditions, can produce very different trends in the wave activity and temperatures (in one the observed features are qualitatively reproduced whereas in the other there is

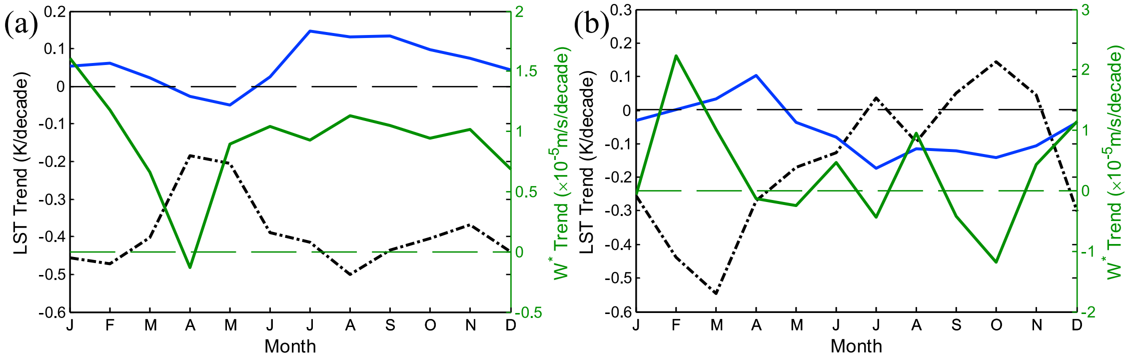

Figure 4. Seasonal variations in the zonal mean trends of 70hPa tropical (20 S–20 N) *w** (green solid) and tropical (black dash-dotted) and high latitude (40 N/S–82.5 N/S) dynamical (solid blue) LST for (a) CMAM-2 and (b) CMAM-3. The correlation coefficients are 0.67 and 0.71 between tropical *w** and LST trends for CMAM-2 and CMAM-3 respectively, 0.46 and 0.39 between tropical *w** and high latitude dynamical LST trends, 0.75 and 0.81 between tropical and high latitude dynamical LST trends.

little agreement). Although there are differences in the seasonality of the trends, in all simulations and observations there is a strong anti-correlation in seasonality of the tropical LST trends and the dynamical component of high latitude LST trends (and hence the trend in wave activity propagating into the stratosphere). There are also significant spatial patterns in southern high latitude trends in later winter-spring, with regions of cooling and warming of comparable magnitude in MSU and CMAM-2 LST.

4. Factors Controlling Tropical Temperature Trends in CMAM Simulations

[27] FSL2010 attributed the observed LST trends described above to a strengthening of the B-D circulation. However, current observational trends for the B-D circulation are not reliable enough [e.g., *Yang et al.*, 2008], and this inference about changes in circulation cannot be tested from observations. This is not the case for the CCM simulations, where the B-D circulation can be diagnosed directly, and trends compared with temperature trends.

[28] To test inferences in the B-D circulation from temperature trends, we compare the trends in the simulated tropical vertical velocity of the residual circulation, *w**, with those in the tropical LST and the dynamical component of the high-latitude LST. A positive *w** trend indicates strengthening of the B-D circulation, and would be expected to lead to a dynamical (adiabatic) cooling in the tropics and dynamical (adiabatic) warming at high latitudes (and vice versa for a negative *w** trend). As shown in Figure 4, the trends in the tropical *w** (green solid curves) in the two CMAM simulations for 1979–2006 are anti-correlated with the corresponding tropical LST trends (black dash-dotted curves) and correlated with their high latitude LST trend dynamical components (blue solid curves). The CMAM-2 *w** trend is positive in all months but negative in April (Figure 4a). The CMAM-3 *w** shows negative trends in January, April, May, July, September, and October (Figure 4b). Therefore, the *w** trends in both CMAM simulations (and also CMAM-1, not shown) are consistent with the wave activity and temperature trends, and support the inference of changes in the B-D circulation from trends in wave activity and temperature.

[29] Although the anti-correlation between tropical *w** and LST trends is consistent with an increased upwelling causing dynamical cooling and a decreasing trend in LST, changes in tropical ozone could also contribute to the tropical temperature trends [e.g., *Forster et al.*, 2007; *Salby*, 2008; *Dall'Amico et al.*, 2010; *Lamarque and Solomon*, 2010; *Randel and Thompson*, 2011]. A decrease in tropical lower stratospheric ozone causes (radiatively) a decrease in tropical lower stratospheric temperatures, and changes in ozone could be driving the temperature trends. As shown in Figure 5a, there is indeed a strong positive correlation between lower stratospheric ozone and temperature trends in the CMAM simulations, consistent with a cooling trend from decreasing ozone. On the other hand, the decreasing ozone is also related to the increase in tropical upwelling (Figure 5c), and it is not possible here to separate the direct dynamical cooling due to increased upwelling (Figure 5b) from the indirect radiative cooling by ozone decreases (that result from increased upwelling). Note that the tropical upwelling has been shifted one month earlier in Figures 5b and 5c, as the vertical residual velocity leads temperature about one month in the annual cycle [*Chae and Sherwood*, 2007]. However, even without this lag the seasonal variations in the temperature and ozone trends are correlated with trends in the tropical *w**. The correlation coefficients between temperature and *w** trends with no time lag are 0.67 and 0.71 for CMAM-2 and CMAM-3, respectively, and those between *w** and ozone trends are 0.61 and 0.56 (compared with the numbers in Figure 5).

[30] Tropical LST also depends on SSTs and the abundance of other greenhouse gases (e.g., CO_2 and H_2O), and trends in these factors could be contributing to the overall trend of tropical LST. However, there are relatively small seasonal variations in tropical SSTs that cannot explain the seasonal LST trends. Also, all simulations use the same SSTs, so the behavior of SST cannot explain the differences between CMAM-2 and CMAM-3 trends.

[31] We now return to the issue of why the trends in the two CMAM simulations are so different. As shown above

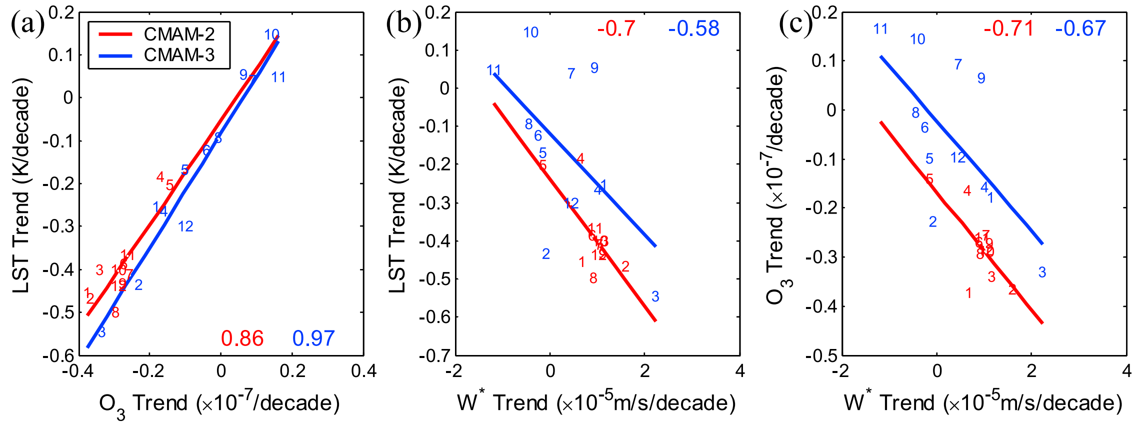

Figure 5. Relation between 1979 and 2006 tropical (20 S–20 N) zonal mean trends in (a) LST and O_3; (b) LST and *w**; and (c) O_3 and *w**. O_3 trend is averaged over 30–70 hPa, and *w** is on 70 hPa. *w** has been shifted one month forward (lag 1) in this comparison. Data points are labeled by months. Straight lines are linear fits between the two variables and their correlation coefficients are also included. CMAM-2 results are shown in red and CMAM-3 results in blue.

the differences can be linked to wave activity entering the stratosphere, so the key question is what is the cause of the CEHF trends. The fact that the CEHF trends can be so different in simulations with exactly the same external forcing indicates that these trends, and as a result seasonal variations in the temperature trends, may not be a robust response to external forcing (such as changes in GHGs and ODSs), and may rather be more the result of internal variability in the model atmosphere.

[32] To examine further the variability in the wave activity entering the stratosphere we consider the variations in CEHF over the whole period (1960 to 2006) of the CMAM REF-B1 simulations. Figure 6 shows the SH high latitude CEHF time series (black dotted curves) for September from CMAM-2 (Figure 6a) and CMAM-3 (Figure 6b). The CEHF trends are shown for the first 28 years (red dashed lines) and last 28 years (blue dash-dotted lines), as well as the whole period (1960–2006; green solid lines). None of these trends are statistically significant at the 5% level based on the *t*-test. In both simulations the trends over the first and last 28 years have similar magnitude but opposite sign. This occurs even though the change in external forcing (GHGs and ODSs) is much larger over the last 28 years than the first 28 years. This indicates that internal 10- to 30-year variability in the wave activity in CMAM is much larger than its sensitivity to external forcing.

[33] As expected from above comparison of wave activity, even when trends are considered over the longer 1960 to 2006 period there is little consistency in the seasonality of temperature trends between CMAM-2 and CMAM-3. Figures 7 and 8 show the results for the above temperature trends analysis applied to the whole period of the CMAM simulations. These results are fairly consistent with those for 1979–2006 (Figures 1e–1h and 3d–3i), except that these trends are weaker and SH high latitude LST trend becomes statistically significant from October to January in CMAM-2. For example, the trend of the CMAM-3 SH CEHF magnitude is negative during July–December over this period (Figure 8d), while its counterpart in CMAM-2 is only negative in November (Figure 8a). This difference leads to dynamical warming in all seasons for CMAM-2 (blue solid curve in Figure 8b and 8c) and dynamical cooling in

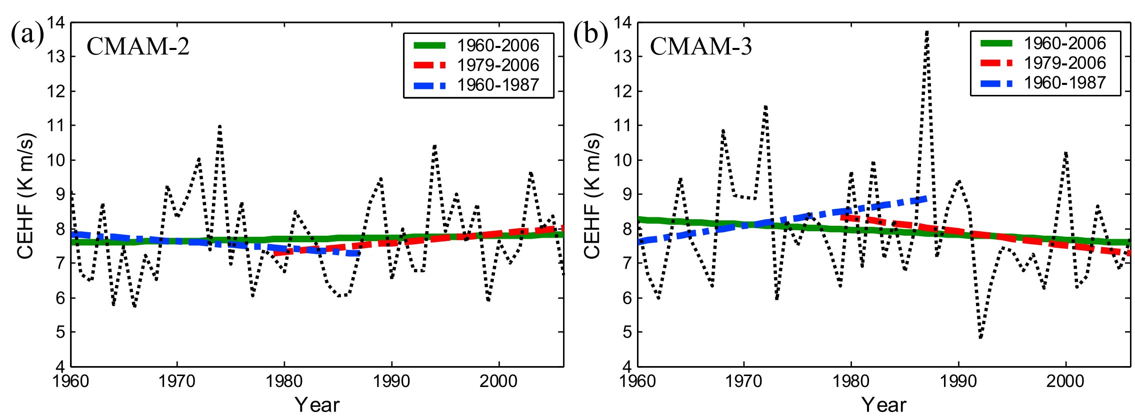

Figure 6. 1960–2006 September SH high latitude (40 S–90 S) CEHF time series (black dotted) for (a) CMAM-2 and (b) CMAM-3. Straight lines represent linear trends over 1960–2006 (green solid), 1979–2006 (red dashed), and 1960–1987 (blue dash-dotted).

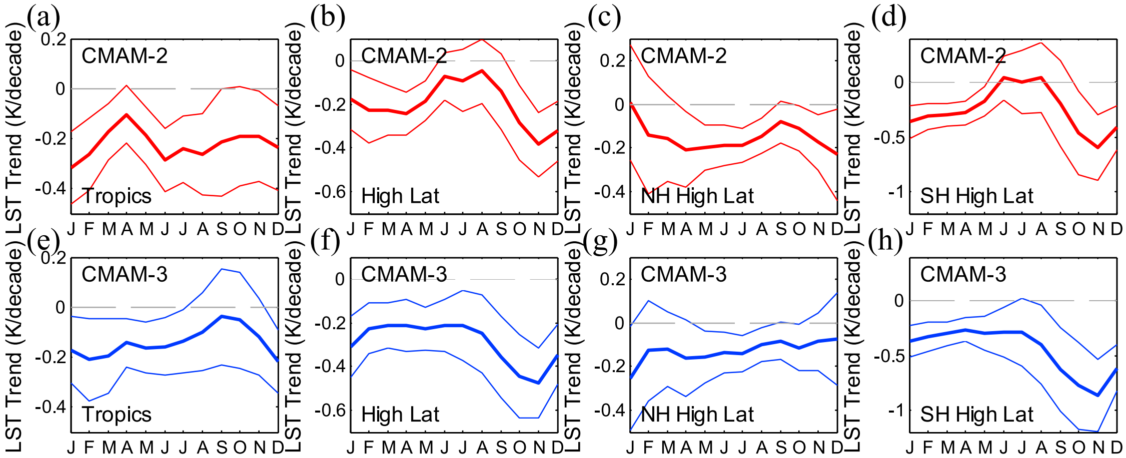

Figure 7. Zonal-mean LST monthly trends (thick) and confidence intervals (thin; 5% significance level based on *t*-test) of CCMVal-2 REF-B1 CMAM-2 simulation for 1960–2006 averaged over latitude bands (a) 20 S–20 N, (b) 40 N/S–82.5 N/S, (c) 40 N–82.5 N, and (d) 40 S–82.5 S. (e–h) Similar to Figures 7a–7d but for CMAM-3.

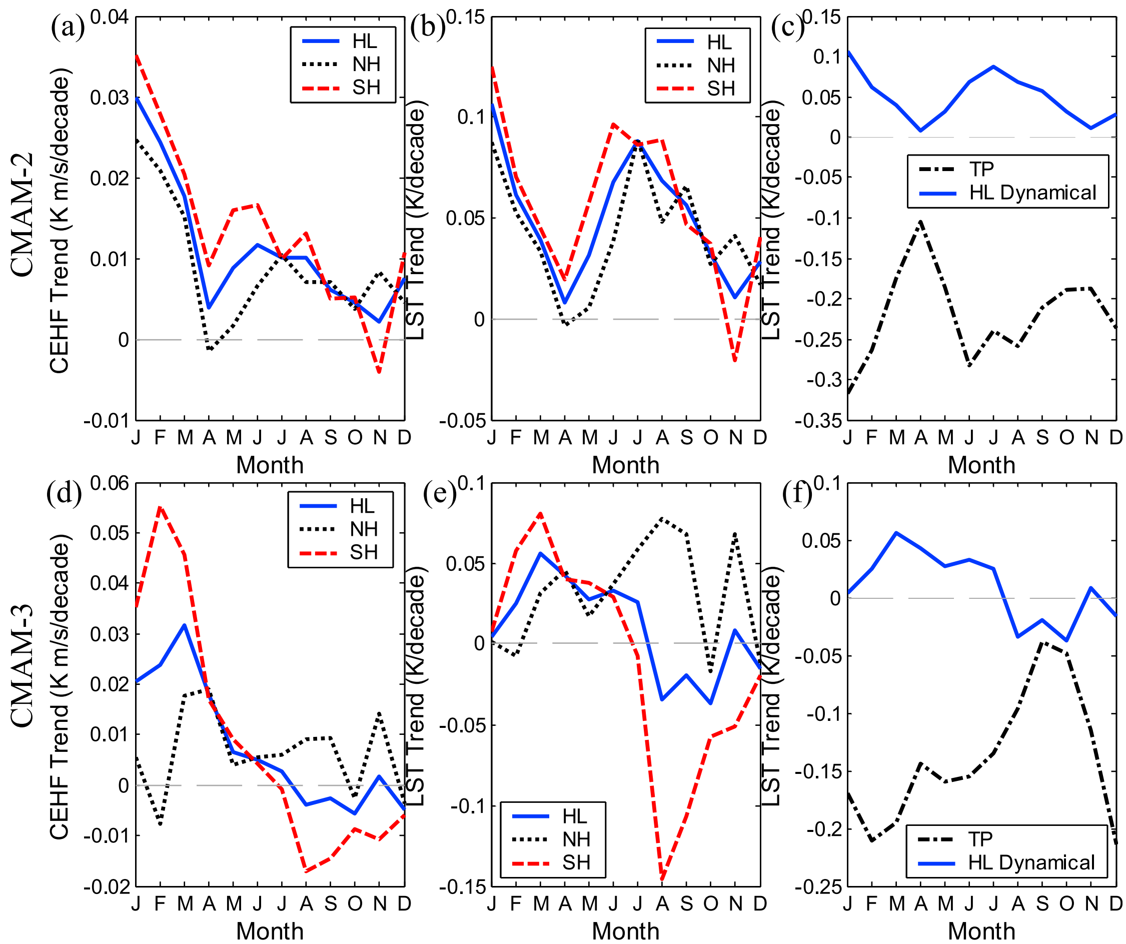

Figure 8. Seasonal variations in the zonal mean trends for 1960–2006 of (a) high latitude (40 N/S–90 N/S) CEHF magnitude; (b) high latitude (40 N/S–82.5 N/S) dynamical LST; and (c) tropical (20 S–20 N) and high latitude (40 N/S–82.5 N/S) dynamical LST for CCMVal-2 REF-B1 CMAM-2 simulation. (d–f) Similar to Figures 8a–8c but for CMAM-3.

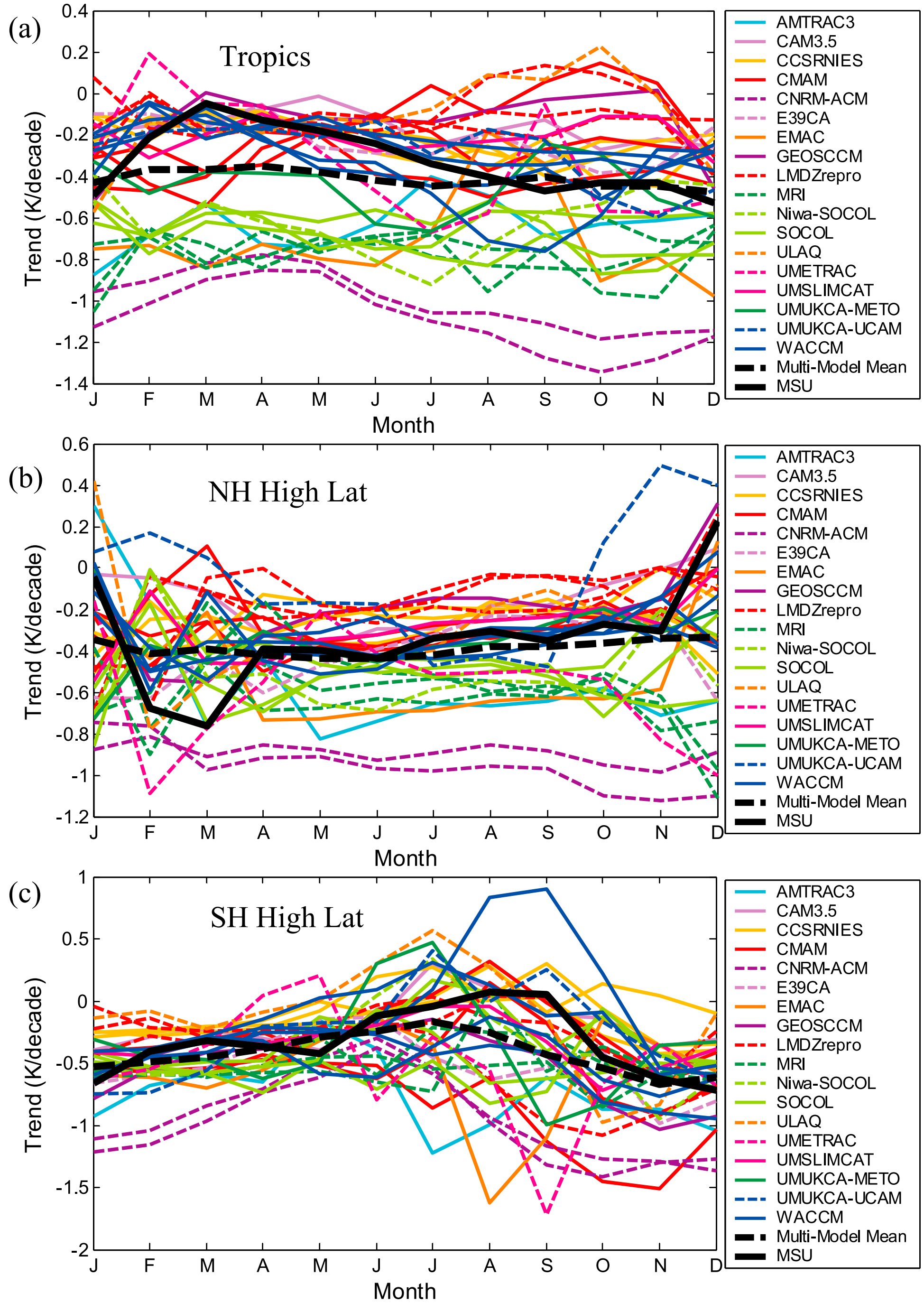

Figure 9. Seasonal cycles of simulated zonal mean LST trends in CCMVal-2 REF-B1 simulations from 1979 to the end of simulation (see Table 1) for (a) 20 S–20 N, (b) 40 N–82.5 N, and (c) 40 S–82.5 S. Multimodel ensemble mean (thick black dashed) is averaged over all ensemble members of individual models with equal weight. MSU LST trends (thick black solid) are also included for comparison.

August–October and December for CMAM-3 (blue solid curve in Figures 8e and 8f).

[34] The above shows that in CMAM the seasonality of LST trends is more sensitive to internal variability than changes in the external forcing over the last 30 years. This may indicate that the observed LST trends may not be dominated by external forcing. However, it is possible that the larger internal variability is due to deficiencies in CMAM. For example, the SH vortex in CMAM is too strong and breaks up too late, while the NH vortex is too warm and variable [*SPARC CCMVal*, 2010]. It is not known how these deficiencies impact the decadal scale variability in the model.

5. CCMVal-2 Models

[35] The above analysis shows that different ensemble members of CMAM can produce very different temperature

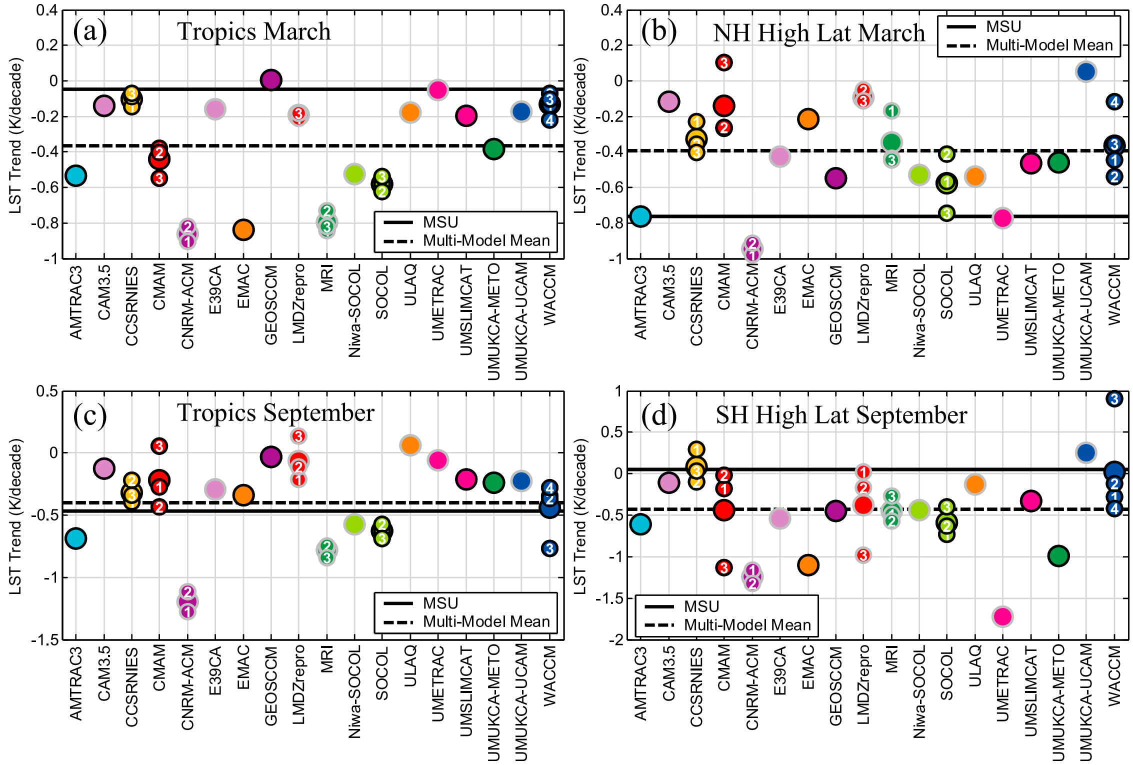

Figure 10. Simulated zonal mean LST trends in CCMVal-2 REF-B1 simulations from 1979 to the end of simulation for (a) 20°S–20°N in March, (b) 40°N–82.5°N in March, (c) 20°S–20°N in September, and (d) 40°S–82.5°S in September. Multi-ensemble members of individual models are shown in numbered small circles and the ensemble mean of each model in large circles. Multimodel ensemble mean (black dashed) is averaged over all ensemble members of individual models with equal weight. MSU LST trends (black solid) are also included for comparison.

trends. We now consider the temperature trends in all 32 CCMVal-2 REF-B1 simulations, and examine variability between models as well as whether this lack of consistency applies to ensemble members of other CCMs.

[36] There are large differences in the tropical and high latitude zonal-mean LST trends among the 32 CCM simulations, see Figure 9 (the 18 different models are shown as different line colors and styles). The magnitude and seasonality of tropical LST trends differs among the simulations, and the multimodel mean shows very little seasonal dependence (multimodel mean tropical LST trend is around −0.4 K/decade for all months, whereas the observed trend varies from near zero in March to about −0.5 K/decade in September). The multimodel mean NH high latitudes trends also show very little seasonal dependence, with few models simulating weak warming in December or large cooling in February–March. In SH high latitudes most of the CCM simulations lack dynamical warming during austral late-winter and spring, and overestimate the zonal-mean high latitude trends.

[37] It is difficult to see the difference between individual simulations (from the same or different models) in Figure 9. These differences are shown more clearly in Figure 10, for NH high latitudes and tropics in March, and SH high latitudes and tropics in September. This figure highlights the large range of simulated trends (−1 to 0.15 K/decade for NH March, −1.8 to 0.9 K/decade for SH September), and differences between the multimodel mean and observed trends. Furthermore, Figure 10 shows that the large differences in zonal-mean trends in CMAM ensemble members also occur for other models. For example, for both months shown the spread of CMAM and WACCM simulations are similar and are about half of the multimodel spread. MRI and SOCOL also show relatively large spread at NH high latitudes in March (Figure 10b) and LMDZrepro shows significant spread at SH high latitudes in September (Figure 10d). The relative spread in the tropics and high latitudes is fairly consistent for the same model (comparing the models with multiple ensembles in Figures 10a and 10c with Figures 10b and 10d), indicating again connection between tropical and high-latitude temperature trends.

[38] There is also a large spread in spatial patterns of the SH high latitudes temperature trends among models. Figure 11 shows the amplitude and phase of zonal wave number-1 component of the temperature trends in October for each of the CCM simulations. The observed SH high latitudes LST wave-1 amplitude peaks in October, and most of the CCM simulations largely underestimate the wave-1 amplitude (Figure 11a). Similar to the zonal mean trend, the wave-1 amplitude and phase vary significantly not only from model to model, but also among ensembles of the same model. The lack of sufficient wave activity might be responsible for the common cold bias and the associated delay in the spring-time break-down of the southern polar

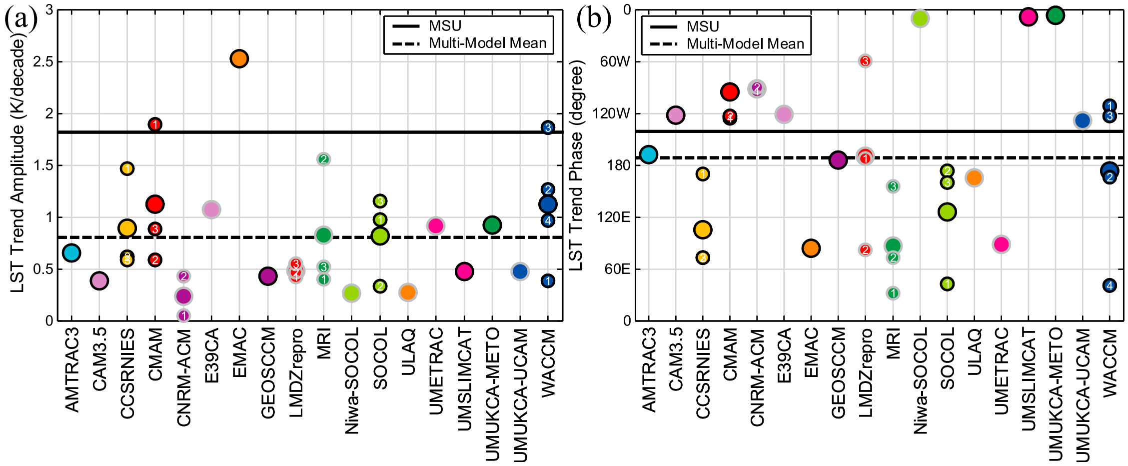

Figure 11. Zonal wave number-1 (a) amplitude and (b) phase of SH high latitudes (50°S–70°S) October LST trend from CCMVal-2 REF-B1 simulations (multimodel ensemble mean in black dashed) and MSU observations (black solid).

vortex in these models [*SPARC CCMVal*, 2010; *Butchart et al.*, 2011; see also *Shaw et al.*, 2011]. The wave-1 phase trends scatter over all longitudes in individual months (e.g., October as in Figure 11b), and their transition from September to October is also irregular in both direction and magnitude. The failure to capture the observed significant transition in the longitudinal location of the warming regions (Figures 2a and 2b) in these simulations (not shown) [see also *Hu and Fu*, 2009] is likely a consequence of the natural variability of the atmospheric circulation.

[39] Although there are generally differences between the simulated trends and those observed, the CCMs are a considerable improvement over the IPCC AR4 simulations analyzed by LFSW2009. The observed local maximum warming trends in September and October south of 45°S are greater than 2 K/decade in SH high latitudes (see Figures 2a and 2b). None of the IPCC AR4 models simulate trends larger than 2 K/decade in September (only one in October) for the same region, and only a fifth of these models simulate an area of warming larger the 1 K/decade (P. Lin, personal communication, 2011). In contrast, over half the CCMVal-2 REF-B1 simulations show regions with warming more than 1 K/decade, and around a quarter have warming above 2 K/decade. The improvement of the CCMs over the IPCC AR4 models is likely due to the well resolved stratosphere and interactive ozone chemistry in the CCMs.

6. Conclusions

[40] We have shown that stratosphere-resolving CCMs can, when forced by observed SSTs, GHGs, and ODSs, reproduce the key features of observed lower stratospheric temperature trends from 1979 to 2006. In particular, CCM simulations can produce regions of cooling and warming of comparable magnitude in the southern polar stratosphere during late winter and spring, and a seasonal variation in tropical trends with minimal cooling in April–May. However, it is also shown that the spatial pattern in southern trends and seasonal variations in tropical trends can vary greatly even for simulations of the same model that differ only in their initial conditions. This is highlighted by two simulations of CMAM (in one the observed features are qualitatively reproduced whereas in the other there is little agreement), but is also found to occur for other CCMs.

[41] The large variation in simulated trends among ensemble members suggests that the observed temperature trends may not be a robust response to external forcing (ozone depletion, increases in GHGs), especially over short periods during which it can be dominated by natural (internal) variability. Presently, the observational record in the SH is not long enough to allow for a separation of forced trends from natural variability [e.g., *Young et al.*, 2012]. Hence, comparison with these trends may not be a fair test of climate models. Even a large number of model runs does not guarantee that the mean of these runs should agree with the observed trends as the reality could be just one realization of many possible responses of the atmosphere to the external forcings. Another implication is that this might further complicate the tropospheric (near surface) climate prediction through stratosphere-troposphere coupling [e.g., *Thompson et al.*, 2005].

[42] Although some aspects of the temperature trends differ between the CCMVal-2 simulations considered, in most simulations the change in the B-D circulation is consistent with that inferred from the seasonality of tropical temperature trends, i.e., increased tropical upwelling during months with tropical cooling, and decreased upwelling when tropical warming. These simulations therefore support the inferences made by FSL2010 regarding changes in the B-D circulation based on MSU trends. The cause of the seasonality of the tropical temperature trends is, however, likely a combination of (direct) dynamical heating and (indirect) radiative effects due to dynamically induced changes in tropical ozone. The quantitative attribution of the total temperature trends between these two factors is of interest for future studies.

[43] **Acknowledgments.** This work was funded by grants from the United States National Science Foundation. We acknowledge the modeling groups for making their simulations available for this analysis, the Chemistry-Climate Model Validation (CCMVal) Activity for WCRP's

(World Climate Research Programme) SPARC (Stratospheric Processes and their Role in Climate) project for organizing and coordinating the model data analysis activity, and the British Atmospheric Data Center (BADC) for collecting and archiving the CCMVal model output.

References

Bodeker, G. E., H. Shiona, and H. Eskes (2005), Indicators of Antarctic ozone depletion, *Atmos. Chem. Phys.*, *5*, 2603–2615, doi:10.5194/acp-5-2603-2005.

Butchart, N., et al. (2011), Multimodel climate and variability of the stratosphere, *J. Geophys. Res.*, *116*, D05102, doi:10.1029/2010JD014995.

Chae, J. H., and S. C. Sherwood (2007), Annual temperature cycle of the tropical tropopause: A simple model study, *J. Geophys. Res.*, *112*, D19111, doi:10.1029/2006JD007956.

Dall'Amico, M., L. J. Gray, K. H. Rosenlof, A. A. Scaife, K. P. Shine, and P. A. Stott (2010), Stratospheric temperature trends: Impact of ozone variability and the QBO, *Clim. Dyn.*, *34*, 381–398, doi:10.1007/s00382-009-0604-x.

de Grandpré, J., S. R. Beagley, V. I. Fomichev, E. Griffioen, J. C. McConnell, A. S. Medvedev, and T. G. Shepherd (2000), Ozone climatology using interactive chemistry: Results from the Canadian Middle Atmosphere Model, *J. Geophys. Res.*, *105*(D21), 26,475–26,491, doi:10.1029/2000JD900427.

Forster, P. M., G. Bodeker, R. Schofield, S. Solomon, and D. Thompson (2007), Effects of ozone cooling in the tropical lower stratosphere and upper troposphere, *Geophys. Res. Lett.*, *34*, L23813, doi:10.1029/2007GL031994.

Free, M. (2011), The seasonal structure of temperature trends in the tropical lower stratosphere, *J. Clim.*, *24*, 859–866, doi:10.1175/2010JCLI3841.1.

Fu, Q., S. Solomon, and P. Lin (2010), On the seasonal dependence of tropical lower-stratospheric temperature trends, *Atmos. Chem. Phys.*, *10*, 2643–2653, doi:10.5194/acp-10-2643-2010.

Hu, Y., and Q. Fu (2009), Antarctic stratospheric warming since 1979, *Atmos. Chem. Phys.*, *9*, 4329–4340, doi:10.5194/acp-9-4329-2009.

Kalnay, E., et al. (1996), The NCEP/NCAR 40-Year Reanalysis Project, *Bull. Am. Meteorol. Soc.*, *77*, 437–471, doi:10.1175/1520-0477(1996)077<0437:TNYRP>2.0.CO;2.

Lamarque, J.-F., and S. Solomon (2010), Impact of changes in climate and halocarbons on recent lower stratosphere ozone and temperature trends, *J. Clim.*, *23*, 2599–2611, doi:10.1175/2010JCLI3179.1.

Lanzante, J. R. (2005), A cautionary note on the use of error bars, *J. Clim.*, *18*, 3699–3703, doi:10.1175/JCLI3499.1.

Lin, P., Q. Fu, S. Solomon, and J. M. Wallace (2009), Temperature trend patterns in southern hemisphere high latitudes: Novel indicators of stratospheric change, *J. Clim.*, *22*, 6325–6341, doi:10.1175/2009JCLI2971.1.

McLandress, C., A. I. Jonsson, D. A. Plummer, M. C. Reader, J. F. Scinocca, and T. G. Shepherd (2010), Separating the dynamical effects of climate change and ozone depletion. Part I: Southern Hemisphere stratosphere, *J. Clim.*, *23*, 5002–5020, doi:10.1175/2010JCLI3586.1.

McLandress, C., T. G. Shepherd, J. F. Scinocca, D. A. Plummer, M. Sigmond, A. I. Jonsson, and M. C. Reader (2011), Separating the dynamical effects of climate change and ozone depletion. Part II: Southern Hemisphere troposphere, *J. Clim.*, *24*, 1850–1868, doi:10.1175/2010JCLI3958.1.

Morgenstern, O., et al. (2010), Review of the formulation of present-generation stratospheric chemistry-climate models and associated external forcings, *J. Geophys. Res.*, *115*, D00M02, doi:10.1029/2009JD013728.

Müller, R., J.-U. Grooß, C. Lemmen, D. Heinze, M. Dameris, and G. E. Bodeker (2008), Simple measures of ozone depletion in the polar stratosphere, *Atmos. Chem. Phys.*, *8*, 251–264, doi:10.5194/acp-8-251-2008.

Newman, P. A., E. R. Nash, and J. E. Rosenfield (2001), What controls the temperature of the Arctic stratosphere during the spring?, *J. Geophys. Res.*, *106*(D17), 19,999–20,010, doi:10.1029/2000JD000061.

Randel, W. J., and A. M. Thompson (2011), Interannual variability and trends in tropical ozone derived from SAGE II satellite data and SHADOZ ozonesondes, *J. Geophys. Res.*, *116*, D07303, doi:10.1029/2010JD015195.

Randel, W. J., et al. (2009), An update of observed stratospheric temperature trends, *J. Geophys. Res.*, *114*, D02107, doi:10.1029/2008JD010421.

Salby, M. (2008), Involvement of the Brewer-Dobson circulation in changes of stratospheric temperature and ozone, *Dyn. Atmos. Oceans*, *44*, 143–164, doi:10.1016/j.dynatmoce.2006.11.002.

Scinocca, J. F., N. A. McFarlane, M. Lazare, J. Li, and D. Plummer (2008), The CCCma third generation AGCM and its extension into the middle atmosphere, *Atmos. Chem. Phys.*, *8*, 7055–7074, doi:10.5194/acp-8-7055-2008.

Scinocca, J. F., M. C. Reader, D. A. Plummer, M. Sigmond, P. J. Kushner, T. G. Shepherd, and A. R. Ravishankara (2009), Impact of sudden Arctic sea-ice loss on stratospheric polar ozone recovery, *Geophys. Res. Lett.*, *36*, L24701, doi:10.1029/2009GL041239.

Seidel, D. J., N. P. Gillett, J. R. Lanzante, K. P. Shine, and P. W. Thorne (2011), Stratospheric temperature trends: Our evolving understanding, *WIRES Clim. Change*, *2*, 592–616, doi:10.1002/wcc.125.

Shaw, T. A., J. Perlwitz, N. Harnik, P. A. Newman, and S. Pawson (2011), The impact of stratospheric ozone changes on downward wave coupling in the Southern Hemisphere, *J. Clim.*, *24*, 4210–4229, doi:10.1175/2011JCLI4170.1.

SPARC CCMVal (2010), SPARC report on the evaluation of chemistry-climate models, edited by V. Eyring, T. G. Shepherd, and D. W. Waugh, *SPARC Rep. 5*, World Meteorol. Org., Geneva, Switzerland. [Available at http://www.atmosp.physics.utoronto.ca/SPARC.]

Struthers, H., et al. (2009), The simulation of the Antarctic ozone hole by chemistry-climate models, *Atmos. Chem. Phys.*, *9*, 6363–6376, doi:10.5194/acp-9-6363-2009.

Thompson, D. W. J., M. P. Baldwin, and S. Solomon (2005), Stratosphere-troposphere coupling in the Southern Hemisphere, *J. Atmos. Sci.*, *62*, 708–715, doi:10.1175/JAS-3321.1.

Ueyama, R., and J. M. Wallace (2010), To what extent does high-latitude wave forcing drive tropical upwelling in the Brewer-Dobson circulation?, *J. Atmos. Sci.*, *67*, 1232–1246, doi:10.1175/2009JAS3216.1.

Yang, Q., Q. Fu, J. Austin, A. Gettelman, F. Li, and H. Vömel (2008), Observationally derived and general circulation model simulated tropical stratospheric upward mass fluxes, *J. Geophys. Res.*, *113*, D00B07, doi:10.1029/2008JD009945.

Young, P. J., S. Solomon, D. W. J. Thompson, K. H. Rosenlof, and J.-F. Lamarque (2011), The seasonal cycle and interannual variability in stratospheric temperatures and links to the Brewer-Dobson circulation: An analysis of MSU and SSU data, *J. Clim.*, *24*, 6243–6258, doi:10.1175/JCLI-D-10-05028.1.

Young, P. J., K. H. Rosenlof, S. Solomon, S. C. Sherwood, Q. Fu, and J.-F. Lamarque (2012), Changes in stratospheric temperatures and their implications for changes in the Brewer-Dobson circulation, 1979–2005, *J. Clim.*, *25*, 1759–1772, doi:http://dx.doi.org/10.1175/2011JCLI4048.1.